Surface and exchange-bias effects in compacted $CaMnO_{3-\delta}$ nanoparticles

V. Markovich,[1] I. Fita,[2,3] A. Wisniewski,[2] R. Puzniak,[2] D. Mogilyansky,[4] L. Titelman,[4] L. Vradman,[4] M. Herskowitz,[4] and G. Gorodetsky[1]

[1]*Department of Physics, Ben-Gurion University of the Negev, 84105 Beer-Sheva, Israel*

[2]*Institute of Physics, Polish Academy of Sciences, Aleja Lotnikow 32/46, 02-668 Warsaw, Poland*

[3]*Donetsk Institute for Physics & Technology, National Academy of Sciences, 83114 Donetsk, Ukraine*

[4]*Blechner Center for Industrial Catalysis & Process Development, Department of Chemical Engineering, Ben-Gurion University of the Negev, 84105 Beer-Sheva, Israel*

(Received 9 September 2007; published 7 February 2008)

Magnetic properties of compacted 50 nm $CaMnO_{3-\delta}$ (CMO) nanoparticles have been investigated. Measurements of ac-susceptibility exhibit upon cooling two magnetic transitions at $T\sim270$ K accompanied by a small spontaneous magnetic moment and a para-antiferromagnetic (AFM) transition at $T_N\sim120$ K, observed previously in bulk CMO. Asymmetric magnetization hysteresis loops observed in applied magnetic fields $H\leq90$ kOe are attributed to an exchange coupling between the antiferromagnetic core and the ferromagnetic (FM) shell of the CMO nanoparticles. This work provides the observation of exchange bias effect in manganite nanoparticles with inverted AFM-core–FM-shell structure, as compared to the typical FM-core–AFM-shell. Effects of surface and exchange anisotropy are also discussed.

DOI: 10.1103/PhysRevB.77.054410 PACS number(s): 75.47.Lx, 75.50.Tt, 75.70.Rf

I. INTRODUCTION

The exchange interaction at the interface between a ferromagnetic (FM) and an antiferromagnetic (AFM) components, resulting in exchange bias (EB) draws a significant interest in recent years due to the intriguing physics and its importance in technological applications.[1] In general, the EB effect occurs when the FM-AFM system is cooled in a static magnetic field through the Néel temperature T_N of the AFM, then an unidirectional anisotropy is induced, leading to a shift of the magnetization hysteresis loop usually in the direction opposite to the direction of the field in which sample was cooled. Most experimental and theoretical studies of EB have been performed for FM-AFM multilayers and for FM nanoparticles embedded in an AFM matrix.[1] The EB effect was also observed in samples involving a ferrimagnet (FI) or a spin-glass (SG) phase (FI/AFM, FM/FI, FI/SG, AFM/SG).[1] Recently, the EB effect was observed in phase separated bulk manganites[2,3] and cobaltites[4] due to intrinsic interface exchange coupling between the FM nanodroplets and AFM (Refs. 2 and 3) matrix or SG (Ref. 4) regions. The EB effect was reported for nanosized $La_{0.7}Ca_{0.3}MnO_3$ with FM core and spin-glass shell.[5] In nanosized AFM manganites the reduction in the superexchange interactions on the surface layer allows the formation of a FM shell, resulting in natural AFM/FM interface.[6] Recently, Rao *et al.*[7] reported the disappearance of antiferromagnetism, the appearance of FM metallic phase for nanoparticles of $Nd_{0.5}Ca_{0.5}MnO_3$, which in bulk form is a robust charge-ordering manganite below 250 K and AFM below 160 K.

In this paper, we present a magnetic study of $CaMnO_{3-\delta}$ (CMO) nanoparticles showing an appearance of weak magnetism at $T\sim270$ K and exchange bias effect below $T_N\sim120$ K in a field cooled (FC) magnetic state. A possible coexistence of three magnetic components: AFM component (cores of nanoparticles), weak FM component due to surface magnetism, and additional weak FM component of the cores, is discussed.

II. EXPERIMENT

Nanocrystalline CMO particles have been prepared by the well known citrate method.[8] The x-ray powder diffraction patterns (XRD) of the samples were collected on Huber Imaging Plate Guinier camera G670 installed on an Ultrax-18 Rigaku x-ray rotating Cu anode source, with a focused monochromator on incident beam providing pure $K_{\alpha1}$ radiation. The nanoparticles were also characterized by transmission electron microscopy (TEM) equipped with energy-dispersive x-ray spectroscopy (EDS) facilities. The XRD pattern of the sample calcined at 600 °C presents the mixture of $CaMnO_3$ and amorphous phase. After annealing at relatively low temperatures (up to 900 °C), the considerable amount of $Ca_2Mn_3O_8$ phase still remains in the product. Annealing at higher temperatures (900–1000 °C) results in the particle size of 45–50 nm. On the other hand, the annealing at higher temperature (>1000 °C) induces fast growth of Mn_3O_4 phase, affecting strongly the chemical composition and off-stoichiometry of obtained powder. In recent study of Boskovic *et al.*,[9] it was reported that nanosized 44 nm $CaMnO_3$ particles were produced by modified glycine nitrate procedure with sintering temperature ~800–1000 °C. After annealing at $T\geq900$ °C in air the almost pure $CaMnO_3$ phase was obtained. The crystal structure of this phase was identified in orthorhombic system of *Pnma* space group. The refined lattice parameters are $a=5.283$ Å, $b=7.457$ Å, and $c=5.268$ Å and are identical to known literature data for $CaMnO_3$.[10] The Rietveld fit for this sample is shown in Fig. 1(a). The average crystallite size estimated from XRD data by means of the Debye-Scherrer equation for samples annealed at 1000 °C is ~50 nm. From the TEM picture, shown in Fig. 1(b) we get approximately 60 nm for single isolated nanoparticles. The additional broadening of the XRD profile can be caused by structural defects of the nanoparticles (such as twins or stacking faults). The similar larger size of nanoparticles evaluated from TEM picture was reported by Rao *et*

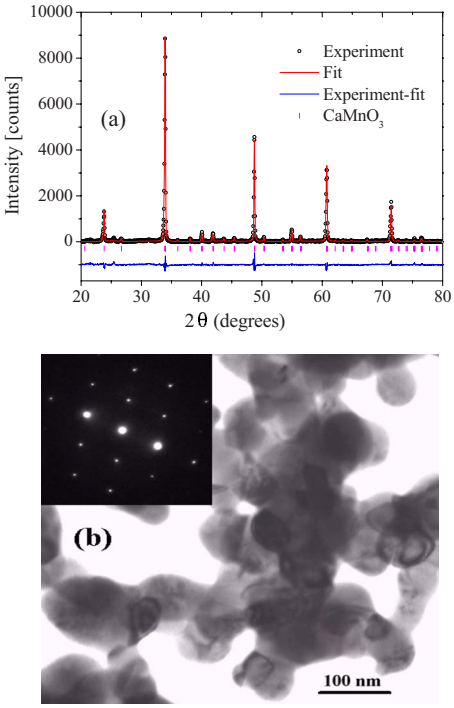

FIG. 1. (Color online) (a) Rietveld plot for CMO sample. The experimental data points are indicated by open circles, the calculated and difference patterns are shown by solid lines. The Bragg positions of the reflections are indicated by vertical lines below the pattern. (b) The TEM bright-field image of the CMO sample. The electron diffraction [inset in Fig. 1(b)] indicates the single crystalline nature of each separated particle.

al.[7] The electron diffraction [inset in Fig. 1(b)] indicates the single crystalline nature of each separated particle. The approximate value of oxygen content determined by EDS analysis is equal to 2.90 ± 0.04. Cylinder-shape samples having a diameter of 1 mm and height of 4.0 mm prepared by compaction of CMO nanoparticle powder under pressure of ~15 kbar at room temperature were used in our magnetic measurements. The measurements of magnetization and ac-susceptibility were performed in the temperature range 5–320 K and magnetic fields up to 90 kOe, using PAR (Model 4500) vibrating sample magnetometer and the ACMS option of the Physical Property Measurement System of Quantum Design.

III. RESULTS AND DISCUSSION

Field-cooled magnetization (M_{FC}) and zero-field-cooled (M_{ZFC}) magnetization curves of CMO sample, recorded at an applied field $H=10$ kOe, are shown in Fig. 2. The sharp change in the magnetization observed at $T_N \approx 120$ K coincides with the AFM transition temperature T_N of $CaMnO_3$.[11–13] In contrast with the results for bulk,[11,12] our CMO sample exhibits a pronounced maximum in M_{ZFC} at $T_{max} < T_N$ and a large difference between ZFC and FC magnetization. It appears also that a minute FM component prevails above T_N, however, due to weak FM signal its transition temperature to paramagnetic state is hardly visible in

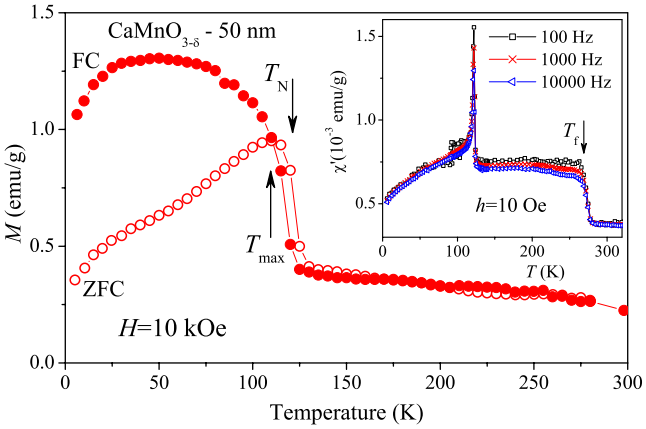

FIG. 2. (Color online) The ZFC and FC magnetization for CMO sample, in $H=10$ kOe. The inset shows the real part of ac susceptibility vs temperature for CMO sample at various frequencies. The probing field has an amplitude of 10 Oe.

high field dc magnetic measurements. Measurements of the real component of the ac susceptibility $\chi'(T)$ of the CMO sample, were carried out at several frequencies between 100 Hz and 10 kHz, see inset in Fig. 2. The results exhibit a steep change at $T_f \sim 270$ K and a sharp peak at $T_N = 122$ K, in the temperature range $125\ \text{K} < T < 265$ K real component $\chi'(T)$ shows a significant dependence on frequency.

Magnetic hysteresis loops were measured at different temperatures after cooling in zero field and after cooling in a field of 15 kOe, see Fig. 3. It appears that small spontaneous magnetization M_0 exists below T_N and a small fraction of it prevails even above T_N. Moreover, almost temperature independent $M_0 \approx 0.06$ emu/g emerges below 270 K. This small moment implies that the FM phase occupies only less than 0.1% of the volume of nanoparticles. Recently, a core-shell structure was proposed[5] to describe the magnetic structure of AFM manganite particles. On this ground we suggest that core of the CMO nanoparticles is AFM below T_N, while the FM shell may embody a SG-like surface layers.[1] As pointed by Nogués *et al.*[1] these SG-like surface layers act as "FM"

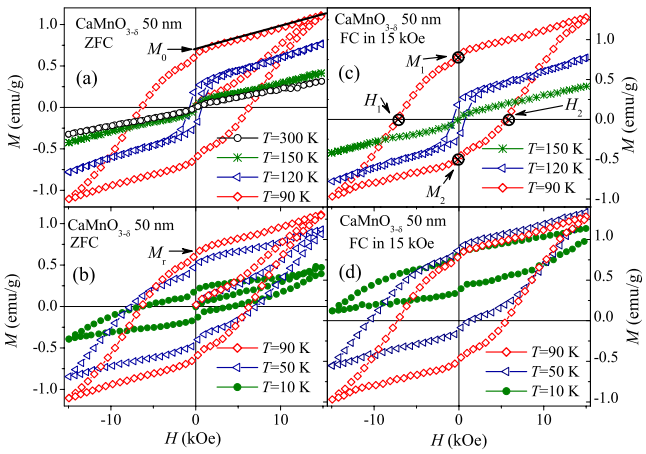

FIG. 3. (Color online) Hysteresis loops of magnetization after ZFC (a), (b) and FC under 15 kOe (c), (d) at various temperatures.

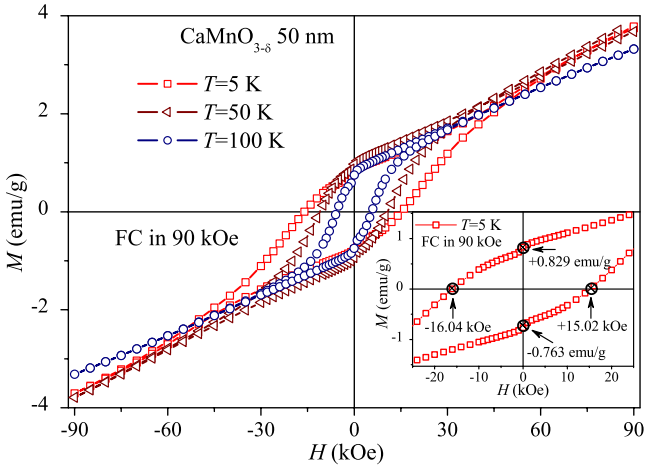

FIG. 4. (Color online) Hysteresis loops of magnetization after FC under 90 kOe at various temperatures. Inset shows hysteresis loop recorded at 5 K in extended scale.

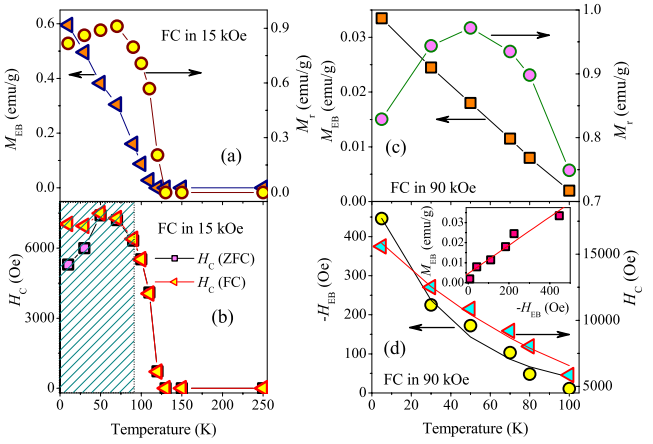

FIG. 5. (Color online) (a) Temperature dependence of M_{EB} and M_r after FC under 15 kOe, (b) Temperature variation of H_C obtained after ZFC and FC under 15 kOe from minor hysteresis loops (Fig. 2). (c) Temperature dependence of M_{EB} and M_r after FC under 90 kOe. (d) Temperature variation of H_{EB} and H_C obtained after FC under 90 kOe (Fig. 3). Inset shows the correlation between M_{EB} and H_{EB}.

on AFM nanoparticles. The maximum value for the spontaneous magnetization observed in our ZFC experiments, is $M_0(T=90\ \mathrm{K})=0.7$ emu/g, see Fig. 3(a). At further decrease in temperature M_0 decreases and approaches a value of $M_0 \sim 0.2$ emu/g ($\sim 0.006\ \mu_B$/f.u.) at 10 K [Fig. 3(b)]. The weak FM moment observed previously in polycrystalline $CaMnO_3$ samples below T_N was attributed to a canting of the AFM moments, or alternatively to a small concentration of defects.[11,12] Though, the most significant asymmetry is seen in the FC magnetization loops [Figs. 3(c) and 3(d)] a difference in the coercive field (H_C) of the ZFC magnetization loops is also noticeable. An open loop was observed at the lowest temperature of our measurements $T=10$ K as can be seen in Figs. 3(b) and 3(d). As generally accepted,[1–3] the magnetic field shift of the hysteresis loop is defined as $H_{EB}=(H_1+H_2)/2$, where H_1 and H_2 are the negative field and the positive field at which the magnetization equals to zero, respectively. The vertical magnetization shift is defined as $M_{EB}=(M_1+M_2)/2$, where M_1 and M_2 are the magnetization at the positive and negative points of intersection with $H=0$, respectively. The asymmetry could be rather determined by the position of the gravity center of the hysteresis loop. Note, that the values of magnetization of the FC loop recorded at 10 K are all positive, when the applied field (15 kOe) is not large enough to redirect the freezing spins.

Additionally, we have recorded hysteresis loops in a wider range of magnetic fields after cooling the sample in a magnetic field $H=90$ kOe (Fig. 4). An examination of these hysteresis loops reveals the existence of a large effective anisotropy, as indicated by a large H_C (~ 15 kOe at $T=5$ K) and a very large irreversibility field ($H_{irr} \sim 70$ kOe at 5 K), below which the decreasing and increasing branches of the magnetization loop separate. A very high H_{irr} could be interpreted as being due to the existence of the SG-like phase.[1]

Figures 5(a)–5(d) summarize the experimental results observed for M_{EB}, H_{EB}, H_C, and remanent magnetization M_r given in Figs. 3 and 4. It appears from Figs. 5(a) and 5(c) that M_r exhibits a similar behavior for both FC at $H=15$ and 90 kOe, displaying local maximum at $T=70$ and 50 K, respectively. On the other hand, M_{EB} after FC in 90 kOe increases monotonically upon decreasing temperature at $T<T_N$. Figure 5(b) presents the $H_C(T)$ of minor hysteresis loops 15-0-15 kOe after ZFC and FC in 15 kOe. It should be noted that the values of H_C extracted from minor loops (Fig. 3) when H_C becomes comparable with FC field (15 kOe) and H_{irr} exceeds the applied field [shaded region in Fig. 5(b)] are a matter of controversy. The same uncertainty exists when one determines H_{EB} and M_{EB} from minor hysteresis loops.[14] It appears, that real values of H_{EB} and M_{EB} may be extracted only from hysteresis loops in which two branches (recorded in increasing and decreasing field) coincide in the high field. Measurements of proper hysteresis loops at high magnetic fields of $H=90$ kOe following FC (Fig. 4) show that H_{EB} and H_C decay exponentially with temperature. Similar decay of $H_{EB}(T)$ and $H_C(T)$ was observed in superlattices consisting of FM $La_{0.67}Sr_{0.33}MnO_3$ and nonmagnetic $SrTiO_3$ layers.[14] The temperature variation of $H_{EB}(T)$ and $H_C(T)$ were described[14] by the following expression: $H_{EB,C}=H_{EB,C}(0)\exp(-T/T_0)$, where $H_{EB,C}(0)$ is the extrapolation of $H_{EB,C}$ to 0 K and T_0 is a constant. Figure 5(d) displays the best fits of the above expression (solid lines) to experimental H_{EB} and H_C. Recently, a relationship between H_{EB} and M_{EB} was analyzed for FM domains immersed in AFM host.[2] Then H_{EB} was introduced as an asymmetry in the activation energy for the backward and forward switching of the particles magnetization over the anisotropy barrier KV (K is the anisotropy constant and V is the volume of the particles).[2] A simple correlation between H_{EB} and M_{EB}: $M_{EB}/M_S \propto -H_{EB}$ was obtained,[2] signifying a direct equivalence of both parameters. Linear correlation between H_{EB} and M_{EB} [inset in Fig. 5(d)] shows that this relationship is valid also for the CMO sample.

Let us discuss the nature of the anomaly in $\chi'(T)$ at $T_f \sim 270$ K (inset in Fig. 2) and the appearance of small FM component at $T<T_f$. In a core-shell structure, the inner part

of the particle, i.e., the core has the same properties as the bulk material, whereas the outer layer, namely, a shell, contains most of the oxygen faults and vacancies in the crystallographic structure. It is well known that $CaMnO_3$ is a *G*-type AFM with a T_N of about 120 K.[11] An oxygen nonstoichiometry in $CaMnO_{3-\delta}$ results in the appearance of Mn^{3+} ions, leading to a formation of FM phase of Mn^{3+}–Mn^{4+} spin clusters at the oxygen vacancies.[13] Electron[15] and neutron diffraction studies[16] have verified the formation of the vacancies superstructures for δ=0.2,0.25, 0.333. Studies of magnetic susceptibility of $CaMnO_{3-\delta}$ polycrystals[15] and $Ca_{1-x}La_xMnO_{3-\delta}$ (x=0,0.05)[16,17] single crystals have shown anomalies of magnetic susceptibility in the temperature range 240–270 K due to formation of FM clusters near defects. It is very relevant to note that the weak surface ferromagnetism is universal feature for any oxide nanoparticles, including nonmagnetic oxides such as Al_2O_3, ZnO, CeO_2 (Ref. 18), and superconducting $YBa_2Cu_3O_{7-\delta}$.[19] These recent studies suggest that ferromagnetism in above materials is due to the exchange interactions between localized electron spin moments resulting from oxygen vacancies at the surfaces of the oxide nanoparticles.[18,19] The anomaly of $\chi'(T)$ at T_f (inset in Fig. 2) and the appearance of M_0 below T_f [Figs. 3(a) and 3(c)] suggest that the magnetic structure of the nanoparticles is comprised of AFM core and FM shell. If the FM shell is as thin as a few lattice units, its spin magnetization may behave as spin-glass-like layer.[1,6]

The high value of H_C observed at low temperatures may be attributed to a large AFM (core) anisotropy and FM (shell)-AFM exchange coupling. The coercivity increases below T_{max} for AFM with relatively small anisotropy, when the rotation of the FM moments results in the drag of the AFM spins irreversibly.[1] However, for a large AFM anisotropy, the FM component decouples because it cannot drag AFM spins, consequently the coercivity is reduced and H_C exhibits a local maximum at $T\sim 60$ K [Fig. 5(b)].[1] Basically, the magnetic energy E of the CMO nanoparticle involves the following terms: $E=E_{Zeff}+E_A+E_{int}$,[20] where E_{Zeff} is the effective Zeeman energy of the FM shell, E_A is the anisotropy energy of the AFM core, and E_{int} is the FM-AFM exchange energy. The magnetic properties of the nanosystem are determined by the interplay of the above energy terms. Upon application of high FC fields ($H\sim 90$ kOe) one may assume that $E_{Zeff} \gg E_A \gg E_{int}$ is high enough to saturate the FM spins along H direction. Then the increase in $M(H)$ can be attributed to the change in the AFM canting angle. An increase in E_A results in monotonic increase of H_C with decreasing temperature. For low temperatures, the remanent magnetization M_r decreases with decreasing temperatures [Figs. 5(a) and 5(c)], while the coercive field H_C rather increases, see Fig. 5(d). Similar behavior observed in amorphous rare-earth alloys[21] and granular CoO layers,[22] has been explained in the frame of the random magnetic anisotropy (RMA) model. According to RMA[21] the remanence decreases monotonically with the increase of anisotropy-to-exchange ratio, while increasing anisotropy leads to the increase of coercivity. We assume that the random anisotropy may originate from randomly oriented CMO nanoparticles with uniaxial anisotropy.

IV. CONCLUSIONS

In summary, 50 nm $CaMnO_{3-\delta}$ nanoparticles were prepared by citrate method. The particles were characterized by XRD, TEM, EDS data. We provide the evidence of surface effects and intrinsic interface exchange coupling in compacted 50 nm $CaMnO_{3-\delta}$ nanoparticles. Our results suggest the coexistence of a predominant AFM phase in the core with a minor FM component at the particle surfaces. The results for compacted $CaMnO_{3-\delta}$ nanoparticles indicate that the magnetic behavior is mainly determined by surface effects, which manifest themselves in high coercive fields, high irreversibility field, and asymmetric magnetic hysteresis loops attributed to the exchange bias effect.

ACKNOWLEDGMENTS

This work was supported in part by the Polish State Committee for Scientific Research under a research Project No. 1 P03B123 30 and by the Israeli Science Foundation, Grant No. 391/07.

[1] J. Nogués, J. Sort, V. Langlais, V. Skumryev, S. Suriñach, J. S. Muñoz, and M. D. Baró, Phys. Rep. **422**, 65 (2005); G. Salazar-Alvarez, J. Sort, S. Surinãch, M. D. Baro, and J. Nogués, J. Am. Chem. Soc. **129**, 9102 (2007).
[2] D. Niebieskikwiat and M. B. Salamon, Phys. Rev. B **72**, 174422 (2005).
[3] T. Qian, G. Li, T. F. Zhou, X. Q. Xiang, X. W. Kang, and X. G. Li, Appl. Phys. Lett. **90**, 012503 (2007).
[4] Y. K. Tang, Y. Sun, and Z. H. Cheng, Phys. Rev. B **73**, 174419 (2006).
[5] M. Muroi, P. G. McCormick, and R. Street, Rev. Adv. Mater. Sci. **5**, 76 (2003).
[6] S. Dong, F. Gao, Z. Q. Wang, J.-M. Liu, and Z. F. Ren, Appl. Phys. Lett. **90**, 082508 (2007).
[7] S. S. Rao, S. Tripathi, D. Pandey, and S. V. Bhat, Phys. Rev. B **74**, 144416 (2006).
[8] M. S. G. Baythoun and F. R. J. Sale, Mater. Sci. **17**, 2757 (1982).
[9] S. B. Bošković, B. Z. Matovic, M. D. Vlajić, and V. D. Kristić, Ceram. Int. **33**, 89 (2007).
[10] H. Taguchi, J. Solid State Chem. **124**, 360 (1996).
[11] J. J. Neumeier and J. L. Cohn, Phys. Rev. B **61**, 14319 (2000).
[12] V. Markovich, I. Fita, R. Puzniak, E. Rozenberg, C. Martin, A. Wisniewski, A. Maignan, B. Raveau, Y. Yuzhelevskii, and G. Gorodetsky, Phys. Rev. B **70**, 024403 (2004).
[13] J. Briático, B. Alascio, R. Allub, A. Butera, A. Caneiro, M. T. Causa, and M. Tovar, Phys. Rev. B **53**, 14020 (1996).
[14] W. Luo and F. Wang, Appl. Phys. Lett. **90**, 162515 (2007).
[15] A. Reller, J. M. Thomas, and D. A. Jefferson, Proc. R. Soc. London, Ser. A **394**, 223 (1984).
[16] S. F. Dubinin, N. N. Loshkareva, S. G. Teploukhov, A. V. Ko-

rolev, E. A. Neifel'd, V. E. Arkhipov, V. D. Parkhomenko, Yu. P. Sukhorukov, and A. M. Balbashov, Phys. Solid State **48**, 1526 (2006).

[17] N. N. Loshkareva, A. V. Korolev, T. I. Arbuzova, N. I. Solin, A. M. Balbashov, and N. V. Kostromitina, Phys. Met. Metallogr. **103**, 251 (2007).

[18] A. Sundaresan, R. Bhargavi, N. Rangarajan, U. Siddesh, and C. N. R. Rao, Phys. Rev. B **74**, 161306(R) (2006).

[19] A. Shipra, A. Gomathi, A. Sundaresan, and C. N. R. Rao, Solid State Commun. **142**, 685 (2007).

[20] A. N. Dobrynin, K. Temst, P. Lievens, J. Marqueritat, J. Gonzalo, C. N. Alonso, E. Piscopiello, and G. Van Tendeloo, J. Appl. Phys. **101**, 113913 (2007).

[21] E. Callen, Y. J. Liu, and J. R. Cullen, Phys. Rev. B **16**, 263 (1977).

[22] M. Gruyters, Europhys. Lett. **77**, 57006 (2007).